An Overview of the LADEE Ultraviolet - Visible Spectrometer

Anthony Colaprete[1], Kara Vargo[1], Mark Shirley[1], Dave Landis[2], Diane Wooden[1], John Karcz[1], Brendan Hermalyn[3], Amanda Cook[1]

[1]NASA Ames Research Center, Moffett Field, Mountain View, CA

[2]Draper Laboratory, Tampa, Florida.

[3]University of Hawaii, Honolulu, Hawaii.

Corresponding Author: Anthony Colaprete, Anthony.Colaprete-1@nasa.gov, 650-604-2918 (phone), 650-604-6779 (fax)

Abstract

The Ultraviolet – Visible Spectrometer (UVS) instrument, which flew on the Lunar Atmosphere and Dust Environment Explorer (LADEE) spacecraft, was one of three science instruments used to characterize the lunar exosphere. UVS is a point spectrometer operating between 230-810 nm and uses its two optical apertures to make observations of the exosphere just above the surface at a range of local times and altitudes, as well as making solar occultation measurements at the lunar sunrise terminator. The instrument was led out of NASA Ames with primary hardware being provided by Draper Laboratories. Final instrument integration, testing and operations were performed by NASA Ames. Over the course of the 140-day LADEE mission, UVS took more than 1 million spectra, providing a unique data set for lunar exosphere gasses and dust.

1 Science Background and Objectives

The Lunar Atmosphere and Dust Environment Explorer (LADEE) is an orbital lunar science mission designed to address the goals of the 2003 National Research Council decadal survey, the Lunar Exploration Analysis Group Roadmap, and the "Scientific Context for Exploration of the Moon" (SCEM) report, and has been recommended for execution by the 2011 Planetary Missions Decadal Survey. The LADEE mission goal is to determine the composition of the lunar exosphere and investigate the processes that control its distribution and variability, including sources, sinks, and surface interactions. It will monitor variations in known gases, such as sodium, potassium, argon and helium, and will search for other, as-yet-undetected gases of both lunar and extra-lunar origin. LADEE will also determine whether dust is present in the lunar exosphere, and reveal the processes that contribute to its sources and variability. The Ultraviolet-Visible Spectrometer (UVS) is one of three science instruments on board LADEE. This manuscript describes the science background, measurement objectives, design, performance, and operations of the UVS instrument.

1.1 Lunar Exosphere: Theory and Observations

Until now the tenuous lunar exosphere has been largely unexplored. After the Apollo program and ground-based observing campaigns, only four constituents of the lunar atmosphere have been positively identified: Ar, He, Na, and K. Argon and Helium are thought to be the main constituents of the exosphere. Sodium and Potassium have been observed in spite of their low abundance due to their strong spectral signatures (e.g., Sprague et al., 1992 and Potter et al., 2000). More recently, observations of sodium at the moon were made by the SELENE spacecraft (Kagitani et al., 2010), although these observations were limited to the night-side hemisphere of the Moon. There are many more species that are expected to exist in the lunar atmosphere that have not yet been confirmed, or lower limits have been established (e.g., Stern et al., 1997, Flynn and Stern, 1996, and Sarantos et al., 2012). The spatial and temporal variability of the lunar exosphere is not understood,

including the sources, release mechanisms, loss processes, and atmosphere/surface interactions. Models exist to probe these relationships (e.g., Hodges, 1980, Sarantos et al., 2012), but there are insufficient data on lunar exospheric variability for validating these models.

Table 1 describes the known and suspected lunar exospheric species (modified from Stern, 1999) that the UVS instrument will address. The densities listed in bold were measured previously via the Apollo 17 Lunar Atmospheric Composition Experiment (LACE) or via ground-based spectrometry. The other densities are approximate near-surface upper limits based on optical/UV remote sensing (Stern, 1999).

There are multiple sources contributing to the lunar exosphere, including the solar wind, the regolith/levitated dust, meteoritic input, and outgassing from the lunar interior. These sources are the reservoirs that supply the constituents. However, the exospheric abundance, spatial distribution, and temporal variations are also determined by the release mechanisms, surface interactions, and loss processes. Sputtering, photon-stimulated desorption, impact vaporization, and outgassing are four processes that can release particles into the lunar exosphere with different energy distributions at release. The height distribution of species in the lunar exosphere varies from species to species, depending on mass and the distribution of release energy. For all elements, density decreases with increasing altitude. However, the constituents typically have ballistic hop heights in the hundreds of km range (e.g., Crider and Vondrak, 2000). Species that make up the lunar exosphere are thus prevalent at 50 km, and will have increasing concentration with decreasing altitude.

Sodium and potassium have already been observed in the lunar exosphere through ground-based observing campaigns and, for sodium, the SELENE spacecraft. Both elements have low abundances in the exosphere, but are detectable due to their strong spectral signatures. Na and K are both volatiles, and are easily ejected from the lunar regolith into the atmosphere due to their low binding energies. However, there are several possible processes capable of releasing these regolith constituents into the exosphere, and the relationship between these mechanisms is controversial (Sarantos et al., 2008). Photon-stimulated desorption (PSD) has been shown to better explain the distribution in the sodium and potassium lunar exosphere. However, a correlation is observed with incident ion flux and the abundance of sodium; in addition, the sodium exosphere has been observed to increase in density during meteor showers. The history of observations and the synergy of contemporaneous orbital and Earth-based observations of Na and K will enable a better understanding of the release mechanisms.

Physical sputtering plays a role in release of the regolith-derived component of the exosphere (Si, Al, Fe, Mg, Ca, O, Ti). Abundances of regolith species differing from stoichiometry may be indicative of the ion sputtering process that ejects the species or subsequent interactions. Impact vaporization also occurs on the Moon, presumably adding meteoric material and regolith material to the lunar exosphere.

1.2 Lunar Dust: Theory and Observations

The dust environment of the Moon has remained a controversial issue since the Apollo era. Visual observations and photographic images from the Apollo command modules, and images from the Clementine mission have been used to indicate the presence of dust at high altitudes above the lunar surface. Most recently, observations with the Lunar Reconnaissance Orbiter star trackers and the Lyman-Alpha Mapping Project (LAMP) spectrograph have continued the search for lunar exospheric dust (Feldman et al., 2014). There are also in situ and remote sensing observations on the lunar surface that indicate dusty plasma processes are responsible for the mobilization and transport of lunar soil.

Television cameras on Surveyors 5, 6, and 7 gave the first indication of dust transport on the airless surface of the Moon (Criswell, 1973; Rennilson and Criswell, 1974). Images taken of the western horizon shortly after sunset showed a distinct glow just above the lunar horizon that was dubbed horizon glow (HG). This light was interpreted to be forward-scattered sunlight from a cloud of dust particles < 1 m above the surface near the terminator. The HG had a horizontal extent of about 3 degrees on each side of the direction to the Sun. Assuming that the observed signal is dominated by diffraction of sunlight, this horizontal extent corresponds to spheres of radius ~5 μm. (Rennilson and Criswell, 1974). The astrophotometer on the Lunokhod-2 rover also reported excess brightness, most likely due to HG (Severney et al., 1975).

Apollo 17 crew reported the appearance of bright streamers with fast temporal brightness changes (seconds to minutes) extending in excess of 100 km above the lunar surface. McCoy and Criswell (1974) argued for the existence of a significant population of lunar particles scattering the solar light. The rough photometric estimates indicated ~0.1 μm sized grains. These drawings were analyzed again (Zook and McCoy, 1991) and most of the earlier conclusions were verified. This study also estimated the scale height of this "dusty-exosphere" to be H ~10 km, and suggested that dust levitation could be observed using ground based telescopes. Recent theoretical models suggest that these observations could result from particles lofted from the lunar surface by electrostatic forces (Stubbs et al., 2006). Images of the lunar limb taken by the star-tracker camera of the Clementine spacecraft also showed a faint glow along the lunar surface, stunningly similar to the sketches of the Apollo 17 astronauts. The interpretation of these images was complicated by the presence of the scattered light from zodiacal dust particles as well as Earthshine. Analysis by Glenar et al., (2011) concluded that excess light could be explained by more typical sources, including Earthshine and internal camera scatter and thus there was no conclusive evidence for lunar HG resulting from exospheric dust.

The Lunar Ejecta and Meteorites (LEAM) Experiment provided the only in situ dust measurement of the lunar surface to date. LEAM was deployed by the Apollo 17 astronauts and started measurements after the return of the landing module; it continued to make observations for about 3 years. LEAM registered an unexpected population of slow-moving, highly charged lunar dust particles. A subsequent experimental study using the LEAM spare showed that the observations were consistent with the detection of sunrise/sunset-triggered levitation and transport of slow

moving (v < 100 m/s), highly charged dust grains. LEAM measurements indicate grain radii on the order of hundreds of microns. Though these observations remained unexplained, they are thought to indicate that the undetected smaller grains could be lofted to high altitudes.

While recent emphasis has been on electrostatic lofting of dust to high altitudes, some fraction of the total dust will also include ejecta from meteoroid impacts. The exact fraction of electrostatic vs. ejecta dust at 50 km is currently unknown. However, analysis of the near-surface Surveyor images indicate that the amount of dust electrically levitated at the terminator is about 10^7 times that expected from dusty meteoroid ejecta (Criswell, 1973). Both electrostatically-lofted dust and secondary impact ejecta originate from the surface.

1.3 LADEE and UVS Objectives

The LADEE mission is intended to explore the tenuous lunar exospheric species and dust above the Moon's surface. To this end the mission has two high-level objectives:

LADEE Objective 1: Determine the composition of the lunar atmosphere and investigate the processes that control its distribution and variability, including sources, sinks, and surface interactions

LADEE Objective 2: Characterize the lunar exospheric dust environment and measure any spatial and temporal variability and impacts on the lunar atmosphere

The UVS instrument supports both of these mission goals, as it is capable of both observing emission by exospheric gases as well as the optical scattering or extinction by exospheric dust. The UVS baseline measurement requirements are:

- Detect resonance scattering emissions of Na, K in the lunar atmosphere with signal-to-noise ratio (SNR) of 5 or better over a single orbit of the LADEE spacecraft. The temporal scales covered shall range from 12 hours to 1 month. The spatial coverage shall be sufficient to resolve variations in Na and K within ±20° of the terminator regions of the Moon.
- Detect resonance scattering emissions, or establish new upper limits for these emissions, with SNR of 5 or better, for the following species over the course of a 100-day mission: Mg, Al, Si, Ti, Fe, and Ca.
- Search for emissions from other, as-yet undetected species not included in the above list, with a SNR of 1 or better over the course of a 100-day mission.
- Perform solar occultation measurements to detect suspended dust particles over an altitude range of 1.5 to 50 km, at a minimum density of 10^{-4} particles/cc, for dust grains 100 nm or larger.
- Perform limb sounding measurements to detect reverse or forward scattered sunlight by suspended dust at 50 km or less, at a minimum density of 10^{-4}/cc.

These measurement requirements were verified prior to flight using laboratory calibrations (Sec 3) and analysis (e.g. Stubbs et al., 2010 and Sarantos et al., 2012). Given the pre-launch understanding of the exosphere and possible dust populations, operations were developed to allow for a variety of observation geometries to address each of these measurement requirements (Sec 4).

2 The Ultraviolet and Visible Spectrometer

2.1 Introduction

The UVS instrument consists of several components integrated into a single instrument. These components include a spectrometer with two foreoptics, a limb telescope and solar viewing optic, optical fibers, integrated mechanical/thermal structure and telescope aperture door. These components and the integrated instrument are described below.

2.2 Spectrometer Design

The spectrometer is "next-generation" design of the Lunar CRater Observation and Sensing Satellite (LCROSS) Visible SPectrometer (VSP). The mechanical components are virtually identical with the VSP, with the only exceptions being mounting features for the integrated circuit boards. The spectrometer is a symmetric f/4 crossed Czerny-Turner spectrometer with a 1 inch aperture (Fig. 2-1). The first spectrometer mirror is spherical in figure, while the oversized camera mirror is toric. The toric figure of the camera mirror allows for a more efficient collection of light from the astigmatic spectrometer, with the spectral image slightly underfilling the 1.4 mm active height of the CCD detector. The 230-810 nm spectrum from the slit is imaged onto a 1044x64 (1024x58 active) pixel Hamamatsu S7031-1006S CCD detector array with integrated thermoelectric cooler (TEC). Each column of pixels is binned within the CCD, delivering a 1x1044 pixel spectrum to the electronics for packaging. The spectrometer contains no moving parts.

At a top level, the LADEE UVS electronics consisted of a few functional blocks (Fig. 2-2) distributed across three printed wiring assemblies. A power supply board takes spacecraft power (28VDC nominal) and converts it to the variety of voltages needed by the remainder of the electronics. A radiation-hard Actel RTAX2000S FPGA provides the timing and triggering needed by the instrument, as well as an embedded 8051 microcontroller. The microcontroller code was contained in and executed from an external 32k x 8 PROM. Internal FPGA RAM was utilized for both microcontroller data (EDAC-protected) and a spectral data FIFO. The microcontroller rovides the UART for the instrument's RS-422 serial interface, as well as the logic for receiving commands from the spacecraft and presenting science data over the serial port. The FPGA feeds a bank of MOSFET drivers that form the clocks needed by the CCD detector. Analog sensor data is conditioned and digitized by a 16-bit 333MHz A/D. The CCD detector temperature is controlled by a built-in single-stage TEC configured to provide cooling only. The detector temperature is monitored by a thermistor integrated within the CCD package. A PID loop implemented in the embedded 8051 microcontroller provides the necessary control of the PID loop, regulating the temperature of the detector to +/- 0.1°C. The UVS electronics also provide over-current protection

for the TEC, as well as monitors for TEC drive current and the temperature of the hot side of the TEC. The UVS telemetry data contains the TEC temperatures and drive currents. This design allowed for the reuse of >90% of LCROSS's VSP FPGA and microcontroller code.

The spectrometer's power varies from 11.2 W to 17 W when the TEC is operated and can reach the peak power consumption of 23.6 W for a short period of time when the spectrometer reaches the set point of its sensor or when the TEC reaches its maximum cooling capacity. Spectrometer power consumption is always limited by the UVS power supply board and does not exceed 23.6 W.

2.3 Telescope and Solar Viewer Design

An approximately 45-cm length, 300-micron core-diameter, bifurcated glass optical fiber attaches the spectrometer to both the telescope and solar viewer fore-optics. Two fibers are contained in this one fiber assembly; they vertically overlap one another at the spectrometer slit but separate to feed into the individual fore-optics. Light is collected from a specific optic by operational constraints: only one optic is illuminated during an observational period.

2.3.1 Telescope

The telescope, a catadioptric design all spherical surfaces (concave primary, convex secondary, plano-convex field lens), presents a 3 inch aperture and a 1 degree field-of-view (Fig. 2-3A). The telescope is optimized for the 250 – 800nm wavelength range. Baffles are incorporated at the secondary mirror mount and primary mirror aperture, and the interior of the telescope tube is bead-blasted to minimize stray light. Mass constraints did not allow for an extended sunshade, however, the secondary mirror spider mounts were beveled away from the entrance aperture by 10° to help minimize scatter into the telescope from surface reflected sunlight (see section 4.5). All interior surfaces are black anodized. A rail is mounted on the underside of the telescope and attaches the telescope to the instrument assembly plate. Finally the telescope has an aperture door assembly (ADM) composing of a delrin cover, a TiNi pinpuller and a locking hinge to protect the telescope optics against contamination sources during the initial mission phases. The ADM was deployed during commissioning prior to the science operations.

2.3.2 Solar Viewer

The solar viewer is a series of six interlocking aperture supports with six concentric aperture disks forming a 1 degree field-of-view (Fig. 2-3B). A ground fused silica diffuser is held in a separate mount and attached to the back of the mount series before the solar viewer connects to the fiber. The diffuser serves two purposes: it attenuates the solar irradiance to a level that can be detected by the spectrometer without saturation and provides an extended spot of light to fill all of the optical modes of the fiber. The entire series of supports is mounted to a rail and held in place by two ring-shaped clamps. The rail mounts the solar viewer to the instrument assembly plate.

2.4 Integrated Instrument Design

The LADEE UVS consists of three components and their supporting electrical and mechanical harnesses as shown in Figure 2-4. The UVS is integrated into the spacecraft on the top radiator deck in the position shown in Figure 2-5.

2.4.1 Instrument Design

The UVS thermal management system was designed to keep the instrument within its operational and survival boundaries throughout all of the mission phases. The system consists of bake-out, operational, and survival heaters, thermostats, temperature sensors, Multi-Layer Insolation (MLI) and radiative surfaces (Fig. 2-6). To minimize dependence between the spacecraft and UVS thermal designs, UVS was design to be thermally isolated from the spacecraft. To thermally isolate the UVS from the spacecraft, each mounting fastener is surrounded by a low thermal conductivity washer (G-10 material) and the instrument wrapped in MLI. Figure 2-6 depicts the UVS MLI used to insulate the instrument.

2.4.2 Spectrometer Thermal Management

A challenge for the design was the thermal maintenance of the spectrometer's thermo-electric cooler (TEC), which cools the CCD detector. The TEC can cool the detector to between 10 and 50°C colder than the spectrometer heat sink. Additionally, during operation, heat is generated at the location of the TEC as well as on the two electronics boards. This heat flows to the bottom cover of the spectrometer, which is also the mounting surface.

To effectively cool the instrument, the spectrometer is inverted and mounted to the bottom of the UVS assembly structure. The opposite side of this assembly area, which faces out from the SC, is coated with a silverized tape and acts the instrument's thermal radiator (Fig. 2-7 and 2-8). The spectrometer bottom cover is thermally coupled to the instrument thermal radiator with 8 bolts and a high thermal conductance gasket (made of Cho-Therm 1671). Additionally, the telescope and solar viewer are also mounted to the side of the assembly structure and thermally coupled with Cho-Therm 1671.

The primary and redundant survival heaters kept the UVS above its survival temperature limit during times of non-operation, such as transfer phase, non-UVS science orbits, or safe-mode. The survival heater is controlled by an independent thermostat and is designed to keep the instrument above -30°C (Fig. 2-6). The bake-out/operational heaters on the spectrometer were used to warm UVS for bake-out (contamination control) and used to warm to operational turn-on temperatures at the beginning of an operational orbit, when necessary. Bake-out/operational heaters are controlled by flight software, based on temperatures recorded by the UVS temperature sensors. Bake-outs were performed shortly after launch (4 days after, >12 hours with the entire instrument over 40°C), during cruise (>20 days with the instrument over 40°C), and shortly after lunar insertion (>24 hours with the instrument over 40°C. These bake-outs were also used to help anneal radiation damage on the CCD. To further mitigate contamination, beginning approximately 5 days after launch and through cruise UVS had a requirement to be kept at least 10°C warmer than the spacecraft surfaces

in the immediate vicinity of UVS. These surfaces were typically less than 20°C. However, because there was sufficient power, it was decided to maintain the UVS in a bake-out state for the majority of the cruise duration.

3 Instrument Environmental Testing and Qualification

The integrated LADEE UVS instrument was subjected to a full environmental test campaign verifying the instrument workmanship and demonstrating instrument performance at the anticipated launch and operational conditions for the LADEE mission.

3.1 EMI/EMC

An electromagnetic interference and compatibility (EMI/C) test was performed at MET Test Labs in Santa Clara, CA to verify the compliance of UVS to mission standards. Conducted emissions testing was performed to characterize the electromagnetic emissions on the UVS power lines, and conducted susceptibility testing was performed to verify the instrument could withstand signals coupled to the power lines. Similarly, radiated emissions tests were performed to verify the magnetic emissions from the instrument were within the acceptable range and radiated susceptibility was performed to verify the instrument could withstand the specified magnetic field over the mission. The specific EMI/C tests are summarized in Table 3-1. The tests were conducted in accordance with MIL-STD-461F.

For the CE102/RE102 and CS101 tests, UVS received a waiver. The test facility had difficulty maintaining a noiseless setup which induced some erroneous peaks in the UVS data. For the remaining tests, UVS demonstrated adherence to the required levels over the frequency range for each test, listed in Table 3-1.

3.2 Vibration

To validate and verify the UVS mechanical design, the instrument underwent a sine burst test, a sine vibration test, and a random vibration test. The sine burst test was performed on the engineering test unit at Quanta Labs in Santa Clara, CA. The sine and random vibration tests were performed on the flight instrument in the ARC engineering evaluation lab (EEL). UVS complied with all levels of testing.

The UVS engineering unit was tested to qualification levels as specified by GEVS, shown in Figure 3-3, therefore the UVS flight unit was tested to acceptance levels. The instrument's fundamental frequency was above 100Hz, as prescribed by the LADEE mechanical specification and requirements document (MSRD), did not show any resonances during testing, and passed all functional tests before, in between each axis, and after the vibration tests.

To minimize contamination during the flight instrument testing, the vibration table was cleaned, covered with Mylar, and had a mobile 10k clean tent positioned over it, which can be seen in Figure

3-4 below. UVS was tested for functionality in a 10k clean tent in between each axis of the vibration testing.

3.3 Thermal Testing

To verify the UVS thermal design and characterize instrument performance, UVS underwent a thermal balance, thermal cycling, and bake-out in a single, extended test. UVS maintained thermal performance throughout the testing, maintained functional performance at each temperature plateau and during thermal transitions and met the outgassing requirement at the completion of the test.

Initially, thermal testing began with a thermal balance to correlate the instrument thermal model to the instrument's performance in vacuum. For this test, the instrument was held at 35°C, 0°C, and -25°C to cover the thermal operational extremes. During thermal balance, stability was defined as a change in temperature that amounts to less than a 5% change in total system energy over an hour. At each balance, the instrument's temperature was held for an hour and maintained stability.

Next, the instrument was thermally cycled to verify successful operation over the required temperature range and induced thermal stresses. UVS was cycled a total of eight times between 55°C and -25°C, with longs soaks at each extreme, including a soak at the survival temperatures. Four of the cycles included four-hour soaks and four of the cycles included twelve -hour soaks to meet the GEVS protoflight standard. A functional test was performed at each cycle soak and during transitions to verify instrument functionality and performance. Additionally, there was a four-hour survival soak at each extreme survival limit, as well as two UVS turn-on tests and two door deployments, one each at the hot and cold operational limits. Finally, bake-out was performed to accelerate the outgassing of volatile material and clean the instrument; outgassing was performed last to leverage the previous hours spent in vacuum. For this process, the instrument was held at 60°C (the UVS upper survival limit) for an extended period of time, with a cold finger on (to collect the contaminants) and a TQCM (Thermoelectric Quartz Crystal Microbalance) on (to monitor the change in the UVS outgassing rate). Bake-out was deemed complete when the out-gassing requirement was met.

A block diagram of the test setup is shown in Figure 3-5. The UVS assembly was mounted on a test stand using the same thermally-isolating mounting interface as with the spacecraft. The test stand coupled the instrument to the chamber and raised the UVS telescope to point out the chamber window. On the outside of that window was an integrating sphere and lamp, which were used to illuminate the telescope during functional testing.

4 Instrument Qualification

4.1 Alignment and Pointing

This section describes the test methods and results for spatial testing of the UVS instrument. During both the ground and flight calibrations, the telescope and solar viewer maintained their

required 1.0 deg co-alignment with the spacecraft reference frame and the 0.15 deg pointing knowledge.

4.1.1 UVS Telescope Fore Optic – Ground Calibration

Prior to integration with the spacecraft, the telescope fore-optic was tested for field-of-view (FOV) position in reference to the instrument's alignment cube. The instrument was mounted to a table about 50 feet from an alignment target and leveled. Using a laser to back-fill the telescope, the FOV was projected across the distance onto the alignment target. The cube normal (CN) vector, defined as the co-aligned laser beam reflection with the laser beam, was projected onto the same target using a second laser. From here, the telescope bore-sight angle with respect to the CN was measured and recorded. Three independent measurements were made to give an estimate of error. In addition to providing the bore-sight vector, these measurements were used to test relative shift in optics before and after environmental testing.

The setup is shown in Figure 4-1. The back-illuminated images were drawn on a card located ~50 feet away and measured with respect to a fixed horizontal line. The angles are depicted in Figure 4-2.

4.1.2 Telescope Boresight – In Flight Calibration

To measure the relative shift in the boresight alignment after launch, the UVS telescope's FOV was swept across the lit lunar limb several times, with a low angular velocity. The slews covered the limb crossing along two orthogonal axes in the UVS telescope's field of view with one done about the spacecraft Z-axis and the other about a vector in the spacecraft X-Y plane. Based on the spacecraft position during this activity and the spectral response of the instrument, the position of the limb crossing was determined and used to calibrate the instrument alignment to the spacecraft frame of reference. This activity was done about both the X and Y axis.

4.1.3 UVS Solar Viewer Fore-Optic – Ground Calibration

The solar viewer is positioned in the same plane, but 12.6 degrees from the telescope fore-optic. This angle offset is to ensure that neither the solar viewer will be looking at the lunar surface during limb observation modes on orbit, nor will the telescope be looking at the lit lunar surface or the sun during occultation mode.

The solar viewer boresight was measured with respect to the CN vector in the X-Z plane in a manner similar to the telescope ground alignment. In the same setup as the telescope alignment, the target was moved closer to the instrument to account for the 12.6 degree offset. The CN vector was marked on the target. Since the solar viewer does not contain internal mirrors that would allow for a back reflection, a small mirror was mounted to a solar viewer ring and screwed onto the front of the solar viewer. This mirrored surfaced created an area to auto-collimate the pointing laser similar to the cube normal measurements. Three independent measurements were made to give an estimate of error and the position of angles is shown in Figure 4-2.

4.1.4 Solar Viewer Boresight – in Flight Calibration

For the solar viewer boresight calibration, the spacecraft performed a series of slews to enable UVS solar viewer crossings of the sun, similar to the telescope boresight calibration, except these slews cross over the entire disk of the sun (as opposed to the partial disk of the moon). These scans were done along two orthogonal axes with 4 complete passes in each axis, shown below in Figure 4-3. Note that the slews were done back and forth along each axis as numbered in the image below. Based on the light curve produced from the instrument during this activity and the corresponding spacecraft position, the vector of the limb was determined and used to calibrate the instrument alignment to the spacecraft frame of reference.

4.2 Wavelength Calibration.

4.2.1 Ground Wavelength Calibration

A Mercury-Argon (HgAr) lamp spectrum was used to perform lab-based wavelength calibrations. 21-lines in the lamp spectrum were used to fit a third order polynomial, correlating wavelength to pixel number. The HgAr lamp was used frequently to trend the wavelength shifts and calibrate the instrument throughout flight I&T at ARC. The polynomial fit was updated during the payload I&T program before and after any environmental testing was performed. Errors in the fits are +/- 0.59 nm. During environmental testing, the instrument demonstrated a shift of up to 3 pixels or 1.8 nm as a result of qualification level vibration tests.

4.2.2 In Flight Wavelength Calibration

During early-mission instrument commissioning, data from the solar viewer boresight calibration activity was used to calibrate the wavelength position for each pixel, similar to the method using the HgAr lamp on the ground. First, a Gaussian response function was fitted to the HgAr lines from the ground data. This response function was convoluted with a standard, high resolution solar spectrum standard from Harvard-Smithsonian Center for Astrophysics (CfA) (Chance & Kurucz 2010) to produce the spectrum that UVS should record when viewing the sun. Using actual spectra from the solar viewer boresight calibration with the solar disk in the FOV, the UVS measured solar spectrum was compared to the convolved CfA standard solar spectrum to determine the wavelength value for each pixel, based on line positions (Table 4-1). The pre and post launch calibrated wavelengths shifted by approximately 1nm as shown in the Table 4-1..

4.3 Dark Calibration

To calibrate for the spectrometer CCD dark current, the instrument's response was characterized for various TEC setpoints and integration times. This calibration was then used to predict the dark current for each spectrum and to remove the dark current from spectra before applying any calibrations.

For this calibration, spectra were recorded at the following TEC set points: -30°C, -25°C, -20°C, -15°C and -5°C and at each TEC set-point, spectra were recorded with the following integration times: 8ms, 100ms, 500ms, 1s, 5s, 10s, 30s, and 60s. This activity occurred both on the ground and

in orbit, and these data sets are used to monitor and trend the dark response of the instrument over the duration of the mission.

In each spectrum, there are blank pixels (pixels 0 – 3 and 1040 – 1043 using zero index notation) and bevel pixels (pixels 4 – 9 and 1034 – 1039). The blank pixels are dark pixels that are optically inactive. The bevel pixels are pixels that are optically active but not entirely back thinned. Pixels 10 – 1033 represent the entire optically active range.

Analyzing the dark response of the spectrometer is a multi-step process of removing the bias and instrument noise to examine the spectra over all TEC set-points and integration times. After the data is recorded and downloaded from the spacecraft individual spectra are "scrubbed" for cosmic rays using a histogram to identify the pixels with counts significantly greater (typically >5-sigma) than the running median in time. These events are flagged and not included in later analysis. Following this cosmic-ray scrub, the median of the last four blank pixels is calculated. The first four have a spike inherent from the spectrometer electronics and are therefore not used. To determine the spectrometer electronics bias offset, the mean of the blank medians is calculated for a given TEC setpoint and subtracted from the individual spectra. Lastly a linear spline fit is made between this mean and pixel 3 of the individual spectra to span the active area of the CCD. The last step in the dark correction of each spectra is to subtract this line from the spectra. Using this corrected data set, the trends evident in hot pixels, thermal dependency, and time can be monitored.

4.4 Scattered Light

4.4.1 Ground tests performed to characterize instrument response to stray light

4.4.1.1 Spectrometer interior stray light rejection

Stray light inside the spectrometer can result from grating shine or reflection off the CCD window. To measure this, the instrument underwent a series of tests to determine if there was any interior stray light and to characterize what stray light was found. At the end of the test, no stray light was found to be higher than 20% of the reference signal.

For the test, a cover was made for the integrating sphere to interface with a series of edge filters and project light through the filter into the telescope's FOV. In the setup, a heat absorbing filter was used to remove any IR from the spectrum and the subsequent 610nm, 630nm, 665nm and 695nm filters were placed in front of the IR filter. For each of the four filters, spectra were recorded and subsequently dark-corrected, time-normalized and averaged over the number of samples recorded. Then, in 5-pixel increments, the integral was calculated for the reference data and the spectra using the 4 filters. From the data, the only stray light seen is at the short wavelengths and this is most likely due to the reference signal being low in that region, diminishing the dynamic range.

4.4.1.2 Off Axis Light Rejection

An off axis light rejection test was performed to gauge the telescope's acceptance of light outside of its FOV. For this test, the UVS instrument was set up on a test bench with a HeNe laser beside it.

The laser was projected onto a target 263.2 cm away and the telescope was positioned so that the laser back reflection was in the FOV. From here, the laser point was stepped in 1.3 cm increments from the center of the telescope FOV to 39.4 cm from the center, so that the angle of incident light varied from 0 to 9.4 degrees from telescope normal.

At each position, twenty spectra were recorded with an integration time that maximized SNR at that position. Following the test, the spectra from each location were averaged, time-normalized and dark-adjusted to give one representative spectrum per each location. Using pixels 710 to 712, which corresponds to 635.5 to 636.6nm (the wavelengths that the laser covered), the integral of the laser response was calculated using the trapezoid rule on both the "in-FOV" spectra and the three "out-of-FOV" spectra. To determine the off axis rejection, each integral of the out-of-FOV data was divided by the integral of the in-FOV data. At angles greater than 1.5° from the center of the telescope FOV, off axis rejection was typically better than 10^4.

4.4.2 Flight measurements to characterize instrument response to stray light

In flight, two sources of stray light have been identified. The first is from direct sunlight impinging directly on the secondary mirror mount at the front of the UVS telescope or on the spacecraft upper deck (radiator) and then onto the mirror mount (3, rays 1 and 3). The sec ond comes from sunlight reflected off the lunar surface and onto the mirror mount (ray 2). The geometry of the UVS operations were adjusted to minimize these sources of scattered light. While operating in "Limb" mode (see Sec 5) lunar and solar scatter surface scatter into the telescope was determined by comparing total signal levels at a variety of surface and solar elongation angles. It was found that when the solar elongation angle was <90°, direct scatter into the telescope was prohibitive. For worst-case surface reflectance scatter, it was found that the total rejection was between 2×10^{-4} and 3.3×10^{-4} at 634 nm, or about a factor of 1.6 times worse than measured in the lab. The discrepancy is due to the difference between the relatively small range of exposure angles in the lab versus what is seen while viewing the lunar limb over a fully illuminated surface. At ultraviolet wavelengths (<330 nm) the rejection is much better, with very little difference between spectra taken at local noon and when the spacecraft is in lunar umbra with no scattering sources present (section 5.4).

4.5 Radiometric Calibration

4.5.1 Radiometric Calibration on the Ground

UVS radiometric calibrations are based on data taken with the SphereOptics integrating sphere. The sphere used for this calibration has both a tungsten-halogen and xenon light source that mix within the integrating sphere to provide uniform illumination at the output aperture over the UVS wavelength range (230.34 – 824.52nm). The sphere has an independent NIST calibrated spectrometer to record the sphere's spectral output in units of radiance ($\mu W/sr/nm/cm^2$) which can then be compared to the UVS recorded spectra in digital number (DN; i.e. counts) to determine a DN/unit-radiance calibration. The data used to calculate the radiance calibration was taken during the instrument's last performance test prior to integration with the spacecraft on July 25, 2012.

To begin this process, both the UVS DN spectra and integrating sphere radiance spectra are dark-corrected by subtracting a recorded dark spectrum from each respective spectrometer at the time of the test. Using the dark-subtracted data, each sphere and UVS spectrum is normalized or divided by its respective integration time in seconds. The sphere-reference data is spline-fit to the UVS wavelength range, to match UVS. From here, the UVS spectrum is corrected for the second order effects from the spectrometer grating. Second order effects are from a small portion of the light at the fundamental frequency (250 – 415nm) being projected onto the CCD at its second harmonic wavelength (500 – 830nm). This correction was generated based on the detector quantum efficiency, the grating efficiency, the mirror reflectivity and the grating reflectivity from recorded data. Finally, the UVS DN spectrum is divided by the sphere radiance spectrum to determine a DN/μW/sr/cm^2/nm value for each UVS pixel.

In summary, the steps needed to apply the radiance calibration to any recorded UVS spectra from flight are:

1. Dark and bias correct the spectra
2. Normalize the spectra by integration time
3. Correct the spectra for second-order transfer effects
4. Apply the radiance calibration

4.5.2 In Flight Radiometric Calibration

To verify radiometric response, UVS spectra of specific lunar surface locations were compared with measurements of the same locations from other missions. UVS activities were planned so that the spectra recorded would have the same incidence and emission angles as spectra from the Moon Mineralogy Mapper (M3) instrument on Chandrayaan-1, and the USGS RObotic Lunar Observatory (ROLO) measurements over the same areas on the lunar surface (work in progress).

4.5.2.1 Moon Mineralogy Mapper

Using STK, the geometry of the UVS activity was mapped to determine the incidence and emission angles to the lunar surface. The M3 data was then filtered for these angles over the same local lunar area and matched to the UVS data over the UVS spectral range. Figure 4-4 shows one area over which UVS and M3 data were compared and Figure 4-5 shows the spectral overlay.

5 Mission Operations and Expected Results

5.1 Instrument Configuration

Although UVS provides a flexible command set and approximately 20 configuration settings, most were left in their default state. Four settings were used during flight:

1. Detector Temperature: the setpoint for the thermo-electric cooler that regulates the detector temperature. Typical values are -30C and -25C.

2. Integration Time: how long to capture photons for a single spectrum. Typical values are 26 msec for solar occultation measurements and 2 sec for limb observations.
3. Streaming Mode Duration: How long to collect spectra before stopping and remaining idle. 20 minutes is a typical value.
4. Streaming Mode Period: The time interval between integration starts. This was normally set to 0 msec, causing the spectrometer to follow each integration immediately with another.

Of these, the first two are the most important and were varied frequently during the mission as the operations team improved its understanding of in-flight instrument performance.

5.2 Nominal Operations

While there are only four internal instrument settings, there are numerous combinations of observing geometries and durations called activity types. Each activity type has a primary science goal and can support other science activities, while each science goal can be supported by multiple activity types. For example, Na and K observations can be derived from spectra taken during "Limb" and "North-South" observation activities (see below). The following section summarizes the viewing geometry and sampling interval for each activity.

5.2.1 Limb Orbit

The limb activity is the principal activity for characterizing lun ar exosphere gases and dust backscatter. In this activity, the UVS telescope is pointed by the spacecraft backward (anti-ram) and just off the moon's limb. These activities are timed so that the telescope points toward the lunar sunrise terminator, the sunset terminator, or toward lunar noon.

Instances of this activity used earlier in the mission consisted of "stares", where the telescope's field-of-view was held a constant attitude above the lunar reference sphere, and "nods", where the field-of-view was swept down to the surface, then up higher than a stare, then back to the stare altitude. Figure 5-1 shows LADEE at the beginning of a limb activity (A) and later at the end (B). At both times, the stare altitude is 20 km. Figure 5-2 illustrates the nod portion of a limb activity. Data collected during nods provides information about the concentration of gasses across different altitudes.

Figure 5-3 illustrates the sizes of the telescope field-of-view (blue) and the solar viewer field-of-view (yellow) and their positions during limb stares. Note that, although light always enters through both apertures, in this configuration, the solar viewer is far from lit surface and the solar viewer's diffusor rejects so much light that all but the brightest sources are irrelevant. The spectrometer is much more sensitive to light entering the telescope aperture, and metadata is provided with the spectra to indicate whether the Sun or Earth are in or near the telescope's field-of-view.

While all limb activities early in the mission contained nods, most performed later omitted them. This change was made initially for limb stares near noon to avoid higher levels of stray light entering the telescope as the field-of-view neared the surface and subsequently for limb activities looking toward the terminators.

5.2.2 Occultation

The occultation activity allows for the characterization of the lunar dust and gases down to very low altitudes (Figure 5-4). The activity is performed with the UVS viewing the sun through its solar viewer while the spacecraft crosses the lunar sunrise terminator (A) and enters the shadow of the moon (i.e., sunset for the spacecraft at B). The orientation of the spacecraft is held constant while it passes into the moon's shadow allowing the UVS to take measurements from a higher altitude down to the lunar surface.

Figure 0-5 shows the relative positions of the solar viewer and telescope fields-of-view during an occultation. Note that the telescope field-of-view is on the surface. The yellow line is the terminator with lit surface on the far side of the line and unlit terrain on the near side. Spectra collected before the telescope field-of-view is sufficiently past the terminator to avoid lit peaks may contain enough photons through the telescope to be relevant. Unfortunately, it was impractical from an operational standpoint to rotate the spacecraft about the solar viewer boresight enough to bring the telescope off the surface.

5.2.3 North-South

The North-South activity is a variant of a limb activity where the UVS telescope field-of-view is pointed either north or south instead of backwards along the orbit track. Like a limb activity, the field-of-view is held a fixed altitude above the lunar reference sphere, and these activities also may contain nods. North-South activities are done to create a 3-D characterization of the lunar exosphere; in particular, to characterize the longitudinal and latitude variations in dust and gas species (Figure 5-6). In this case, the spacecraft maintains a near constant attitude relative to the sun. The telescope field-of-view is steady above the limb although the solar viewer field-of-view moves around some. However, the solar viewer FOV does remain off of the surface for the duration of these activities.

5.2.4 Sodium Tail

The sodium tail activity is a limb stare in the lunar night that makes measurements of the moon's sodium tail. The results will be corroborated with other similar science measurements made on other missions.

5.2.5 Forward Look

The Forward Look activity provides observations in a geometry which maximize signal from any dust that may be in the instrument FOV. Small dust grains tend to scatter most strongly in the forward direction (that is anti-sun, or near 180 degrees of phase angle relative to the light source). Forward scattering can be between 20 to 100x greater than backscattering (0 degrees relative to the light source). The forward look geometry provides similar viewing conditions to what the Apollo astronauts had from orbit, as the command module came up on spacecraft sunrise (over the lunar sunset terminator). In normal spacecraft-RAM limb observations, UVS takes measurements in the backscatter orientation over the sunset terminator. The Forward Look direction performs the same Limb observations, including nods, but with UVS pointed in the forward (RAM) direction. These

observations would provide maximum sensitivity to dust at the sunset terminator. Also, measurement of both the forward and backscatter contribution from putative lofted dust will help provide constraints on particle size and shape.

5.2.6 Almost Occultation

Almost Occultation activities are a variant on occultations that hold the solar viewer's field-of-view slightly off of the sun while putting the telescope's field-of-view in the same position relative to the sun as it is during normal occultations. Figure 5-7 illustrates an Almost Occultation (compare this with Figure 5-5). Almost Occultations were performed to study the impact of stray light into the telescope on normal occultation measurements.

5.2.7 Almost Limb

Almost Limb activities use the telescope to search for dust close to the surface, complementing occultations which use the solar viewer for the same purpose. They are called Almost Limb activities because they place the telescope's field-of-view above the limb just after the spacecraft enters umbra like some limb activities. They are different, however, in that the spacecraft is held in a fixed (inertial) attitude and the telescope field-of-view moves with the sun, approaching and crossing the limb (effectively setting) shortly after the sun sets (Fig. 5-8). This is done to hold constant the contribution from Zodiacal Light, which is within the field- of-view and behind any forward scattered light from low dust.

5.3 Instrument Planning and Real-time Operations

Instrument operations and activity planning took place in the instrument operations center (IOC) located in building N240 at NASA Ames Research Center. In the IOC, the data from the spacecraft was displayed in telemetry pages whenever the spacecraft was in view and telemetry was streaming from the science operations center. Available telemetry included a good overview of the spacecraft as a whole – power, propulsion, communications, thermal, payloads, and software, and UVS power, temperatures and heater state.

To operate the instrument, command sets were arranged into a relative time sequence (RTS) that exectued specific commands sequentially. Each RTS was tested on a hardware-in-the-loop simulator before first use. To incorporate an RTS into the larger spacecraft command sequence, the planning tool LASS (LADEE Activity Sequence Scheduler) was used (Fig. 5-9). The spacecraft team would provide the individual instrument team an activity allocation for a 3 – 5 day period where the instruments would insert the desired RTSes and then in the science operations working group, these instrument plans would be combined into one larger science plan. From here, the science plan would receive updated ephemeris from the spacecraft and any updates to the spacecraft RTSes before being turned into a absolute time sequence (ATS). The ATS was uploaded to the spacecraft and provided each RTS with an absolute start time to run.

5.4 Expected Results

Prior to flight, ground calibrations and analyses were used to determine the expected performance of the UVS system for both "Limb" and "Occultation" activity types. These results can be extended in a general sense to other activity types given their viewing geometries and expected signal strengths (e.g., for a particular gas species or dust column).

For each of the gas species in the UVS Level 2 requirements (Sec 1.3) the expected integration time to reach an SNR=5 was calculated given the specified concentrations in the Level 2 requirement (Table 1) and laboratory radiance calibration. These calculations were made for a fixed g-factor (Table 1), and while this is appropriate in most cases, in those cases where the g-factor may vary substantially (Sarantos et al., 2012) there was significant margin in total integration (e.g., Ti).

Figure 5-10 shows the calculated SNR for the exospheric species at the concentrations specified in the Level 1 requirements (Table 1) for several cumulative integration times. The calculations were made using a laboratory measured noise-equivalent power for a detector at -20°C, but modified to account for in-flight measured increases in noise from radiation effects (Sec 3.5). Based on these analyses, new upper limits can be set for most species within a single UVS orbit. That said, some spectra during a particular activity may not be as applicable due to observational constrains (e.g., pointing and off-axis scattering limits).

The expected SNR of any particular gas will depend on its spatial distribution. As listed in Section 1.3, a UVS goal is to measure the spatial variation of sodium and potassium. Spatial variations are measured by measuring concentrations at each of the two terminators and during the noon activity. Figure 5-11 highlights the UVS's capability of measuring sodium based on the UVS "Noon" limb stare with a nod maneuver. These simulations assumed sodium varied as the square of the cosine of the solar longitude and as the cosine of the selenographic latitude. Panel A is the limb and nod activity as a function of time. Panel B is the same activity but as a function of the telescope bore sight altitude. The peak SNR are at the limb stare altitude of 18 km. Panel C is the same activity simulation, but this time plotted as a function of solar longitude. Since the UVS is looking in the anti-velocity direction, the graph is essentially the mirror image of the first.

Similar analysis was carried out for dust observations. Stubbs et al., (2010) carried out a number of predictions for the total dust scatter, or lunar horizon glow (LHG), and possible background contributors, including zodiacal light (ZL). These studies indicated that at decreasing solar elongation angles, LHG becomes a decreasing fraction of the total signal, with the majority of signal contributed by ZL. Possibly distinct color differences between ZL and LHG may help to separate the two contributions. Additional studies were carried out internal to the UVS team which included forward and backward scattered radiance calculated using DISORT (Discrete Ordinates Radiative Transfer). Dust clouds with various mean radii were used to calculate optical depths. For each mean radius a log-normal distribution of dust grains was assumed with a variance of 1.5. Optical coefficients were calculated using Mie theory and indices of refraction for SiO_2. Total transmission through a dust cloud was also calculated using DISORT to support UVS occultation measurements.

Figure 5-12 shows results for these dust simulations for forward and backward scattering radiances and the UVS NEP. Also shown in Figure 5-12 is the expected off-axis light scattering contribution from fully lit lunar surface scattering into the limb-viewing telescope as the telescope holds a fixed stare point 50 km above the surface. For this estimate the lab measurement at 634 nm was used to scale modeled surface reflectance. Figure 4-6 also shows the modeled surface reflectance, scaled by estimates of the in-flight measured rejection at 634 nm at 20 km and 50 km. During UVS activities in which UVS is positioned over lit lunar surface, off-axis lunar surface scatter limits dust measurements to concentrations above 2×10^{-4}/cc (assuming a particle radius=100 nm). To minimize the effects of lunar surface scattering, UVS activity times were adjusted in flight such that illuminated atmosphere was observed while the UVS instrument was positioned over dark (including SC in lunar umbra) or dimly-lit lunar surfaces at each of the two terminators (both in forward and backward views). In these instances the dust detection limit is determined by the UVS NEP.

Solar Occultation measurements have the benefit of having very high SNR, with typical SNR greater than 500 in a single 15-30 msec integration time. The high sample rate allows for vertical sampling, as the sun appears to set, of approximately the angular size of the solar disk up until the solar disk touches the lunar limb. For a solar disk angular size of 0.52 deg this results in an approximate 3.7 km vertical sampling for a spacecraft at an orbit altitude of 50 km. The duration of the occultation is approximately 2.2 minutes (from 35 km to the lunar limb, although it varies by approximately 0.2 minutes from activity to activity) giving a vertical rate of motion of about 0.23 km per sec. At a sample rate of 25 msec, the motion of the solar disk is greatly over resolved and thus allows for additional co-adding of spectra to build SNR further. Figure 5-13 shows the calculated extinction for spherical grains with radii of 10, 100, and 1000 nm, at a concentration of 10^{-4} per cc. The same grain size distribution and optical constants were used as before (Fig. 5-13); however, DISORT was run in transmission mode (viewing the sun through a plan parallel slab).

6 Summary

The LADEE UVS instrument is a simple, robust system that allows for a variety of different observation options, both for dust and gases. UVS provides unique observations of sodium and potassium, able to monitor these gases at a variety of local times over several lunations. These observations combined with observations from the other LADEE instruments and models of the lunar exosphere will provide constraints on the relative importance of impact vaporization, sputtering and PSD. Likewise, UVS provides either measurements or new upper limits on a variety of gas species and dust. The operation of the UVS instrument was relatively complex, having to coordinate SC attitude maneuvers to point the instrument foreoptics with instrument operation. Cooperation with the Project Science and other instrument operation planners was critical. Use of the LASS scheduling tool, with a 2-4 day tactical planning cycle, proved very successful, approximately doubling the number of observations made by UVS over what was expected prior to launch. Likewise timing of operations was quickly adjusted to minimize scattering and, later in the mission, further adjusted to allow for increased cooling of the CCD, minimizing thermal noise.

Acknowledgements

We are grateful for the opportunity to participate in the LADEE Mission and to all the people who made UVS and flight operations possible. This effort was supported by the NASA Science Mission Directorate Lunar Quest Program.

References

Crider, D. H. and R. R. Vondrak. The solar wind as a possible source of lunar polar hydrogen deposits, J. Geophys. Res., 105 , E11 , 26773 (2000)

Criswell, D. R., Horizon-glow and the motion of lunar dust, in: Photon and Particle Interaction in Space, ed: R. J. L. Grard (Dordrecht: D Reidel), 545, (1973.).

Feldman,P. D., D. A. Glenarb, T. J. Stubbs, K. D. Retherford, G. R. Gladstone, P. F. Miles, T. K. Greathouse, D. E. Kaufmann, J. W. Parker, S. A. Stern, Upper limits for a lunar dust exosphere from far-ultraviolet spectroscopy by LRO/LAMP, *Icarus*, **233**, 106–113, (2014)

Flynn, B. C. and S. A. Stern, A Spectroscopic Survey of Metallic Species Abundances in the Lunar Atmosphere, *Icarus*, **124**, Issue 2, 530-536, (1996)

Glenar, D. A., T. J. Stubbs, J. E. McCoy, R. R. Vondrak, A reanalysis of the Apollo light scattering observations, and implications for lunar exospheric dust, PSS, Volume 59, Issue 14, 1695-1707, (2011)

Hodges, R. R., Jr., Methods for Monte Carlo Simulation of the Exospheres of the Moon and Mercury, *JGR*, **85**(A1), 164–170, (1980)

Kagitani, M. M. Taguchi, A. Yamazaki, I, Yoshikawa, G. Murakami, K. Yoshioka, S. Kameda, S. Okano, Variation in lunar sodium exosphere measured from lunar orbiter SELENE (Kaguya), *PSS*, **58**, Issue 12, 1660-1664, (2010)

McCoy, J. E., Criswell, D. R., Evidence for a high latitude distribution of lunar dust, Proc. Lunar Sci. Conf. 5th, 2991, (1974)

Potter, A. E., R. M. Killen, T. H. Morgan, Variation of lunar sodium during passage of the Moon through the Earth's magnetotail, *JGR*, **105**, E6, 15073-15084, (2000)

Rennilson, J. J., Criswell, D. R., Surveyor observations of lunar horizon glow, The Moon 10, 121, (1974)

Sarantos, M., R. M. Killen, D. A. Glenar, M. Benna, T. J. Stubbs, Metallic species, oxygen and silicon in the lunar exosphere: Upper limits and prospects for LADEE measurements, *JGR*, **117**, Issue A3, CiteID A03103, (2012)

.

Severny, A. B., E. I. Terez, and A. M. Zvereva, The measurements of sky brightness on Lunokhod-2, The Moon 14, 123-128, (1975)

Sprague, A. L., R. W. Kozlowski, D. M. Hunten, W. K. Wells, F. A. Grosse, The sodium and potassium atmosphere of the moon and its interaction with the surface, *Icarus* **96**, 27-42, (1992)

Stern, S. A., J. W. Parker, T. H. Morgan, B. C. Flynn, D. M. Hunten, A. Sprague, M. Mendillo, M. C. Festou, NOTE: an HST Search for Magnesium in the Lunar Atmosphere, *Icarus*, **127**, Issue 2, 523-526, (1997)

Stern, A. S., The Lunar Atmosphere: History, status, current problems, and context, *Reviews of Geophys.,* **37**, 453, (1999)

Stubbs, T. J., Vondrak, R. R., Farrell, W. M., A dynamic fountain model for lunar dust Advances in Space Research 37, 59-66, (2006)

Stubbs, T. J., D. A. Glenar, A. Colaprete, D. T. Richard, Optical scattering processes observed at the Moon: Predictions for the LADEE Ultraviolet Spectrometer, *PSS*, **58**, Issue 5, 830-837, (2010)

Zook, H. A., E. McCoy, Large scale lunar horizon glow and a high altitude lunar dust exosphere, Geophys. Res. Lett. 18, 2117, (1991)

Table 1 – LADEE UVS species called out in L1/2 requirements with examples of approximate line centers (most species have more than one potential line (Sarantos et al., 2012), g-factor and assumed L1 pre-LADEE upper limits or average measured value (in the case of Na and K).

Species	Emission/ Absorption Center (nm)	g-factor (sec^{-1})	L1 Upper Limits (#/cc)
OH	309 / 315	0.00047	1.E+06
Al	394.4	0.0285	55
Ca	422.7	0.49	-
Fe	271.9	0.238	380
K	769.9	1.94	17
Na	589	0.307	70
Si	251.5	0.0021	48
Ti	504	0.680	1
Ti	363.65	0.087	1
Mg	285.2	0.032	6000
O	558	2.0E-02	1000
H2O+	654	0.0065	100

Table 0-1. The specifications and corresponding MIL-STD-461F sections from the UVS EMI/EMC test

MIL-STD-461F Paragraph No.	**Test Description**
5.4	CE101 Conducted Emission, Power Leads, 30 Hz to 10 kHz
5.5	CE102 Conducted Emission, Power Leads, 10 kHz to 10 MHz
5.17	RE102: Radiated Emissions, Electric Field, 2 MHz to 18 GHz
5.7	CS101: Conducted Susceptibility, Power Leads, 30 Hz to 150 kHz
5.20	RS103: Radiated Susceptibility, Electric Field, 200-900 MHz at 200 V/m, and 5.0 – 6.0 GHz at 60 V/m.

Table 0-1. The in-flight wavelength calibration used standard solar lines convolved with the UVS spectral response to compare to actual spectra from the solar viewer boresight calibration.

Data Recorded November 1, 2013					
Pixel	Measured λ (nm)	Δλ From Pre-Flight	Pixel	Measured λ (nm)	Δλ From Pre-Flight
77	274.276	0.896	278	393.306	0.834
85	279.638	0.832	284	396.801	0.839
94	284.994	0.823	342	430.480	0.888
130	305.770	1.392	439	486.376	0.973
135	309.323	0.798	493	517.275	1.008
218	358.228	0.801	739	656.299	0.822
261	382.806	1.407	991	794.681	1.124

Cubic Fit: $\lambda[nm] = a_0 + a_1 x + a_2 x^2 + a_3 x^3$; *x = pixel number from [0:1023]*	
Intercept:	2.28659E+02
First Coefficient:	5.99468E-01
Second Coefficient:	-2.75462E-05
Third Coefficient:	-1.00518E-09
Regression Fit:	0.9999976

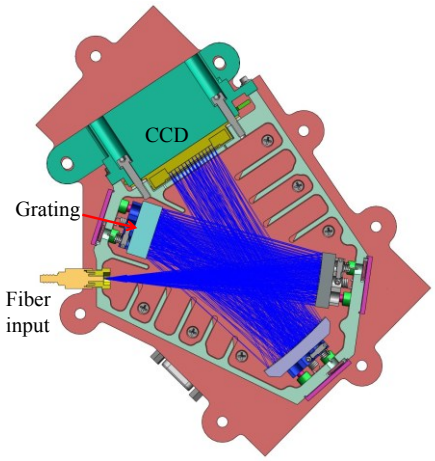

Figure 2-1. Shown is the UVS spectrometer optical layout with ray trace.

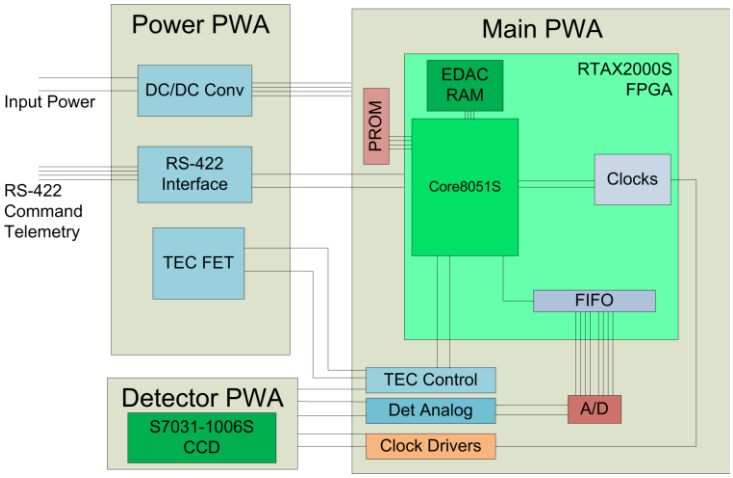

Figure 2-2 Shown is the UVS electronics block diagram with key components and interfaces.

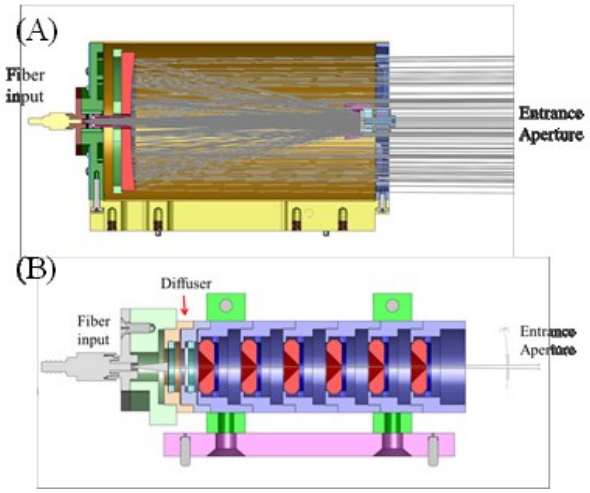

Figure 2-3 Shown are the optical/mechanical layouts for the (A) UVS Limb Telescope and (B) the UVS Solar Viewer

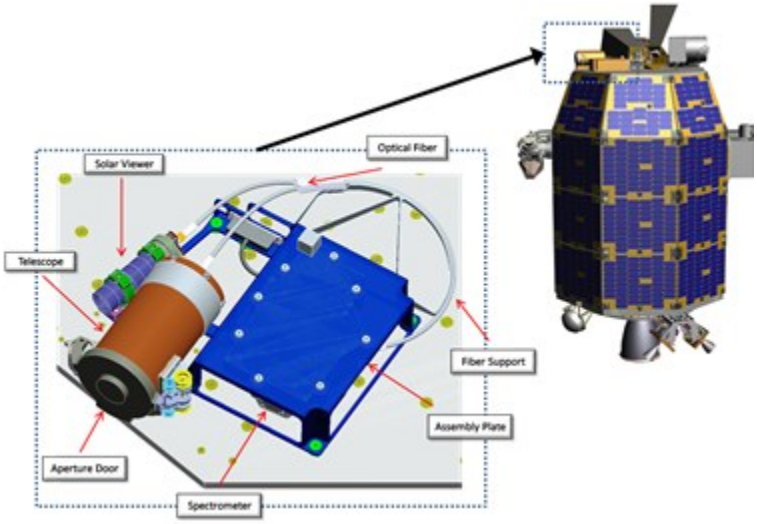

Figure 0-4 The UVS instrument assembly is mounted as one component on the radiator deck at the top of the LADEE spacecraft.

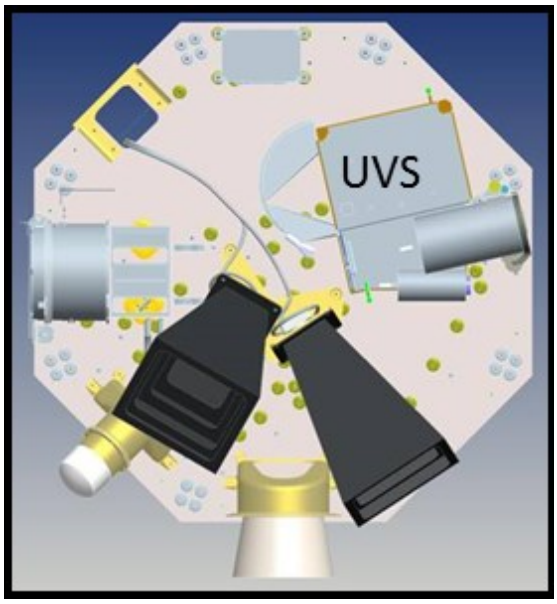

Figure 0-5 Shown is the location of UVS mounted on the spacecraft top radiator deck.

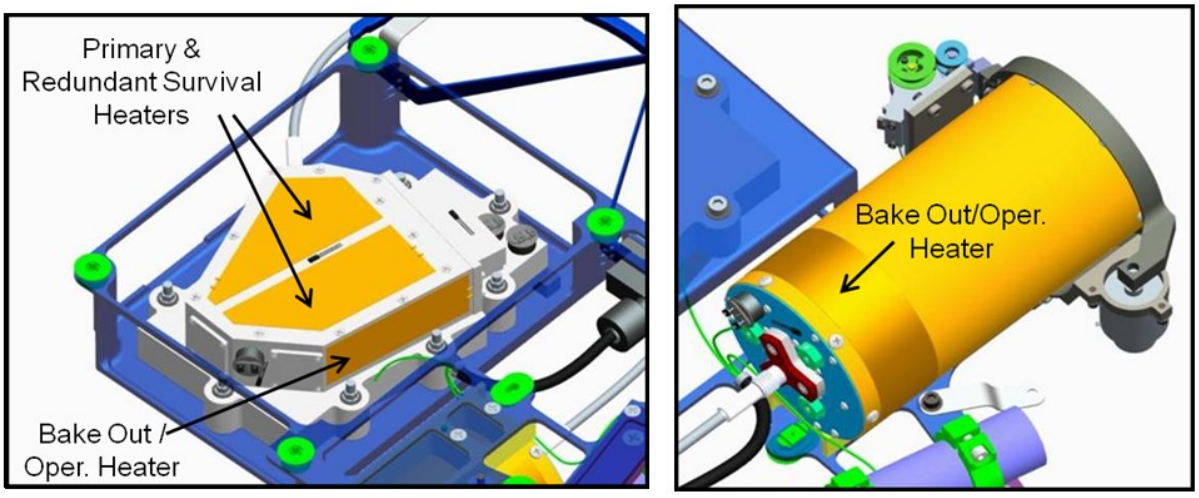

Figure 0-6. The spectrometer survival and operational heaters are mounted to the spectrometer housing and positioned around the internal optics (left). The telescope operational heater wraps around the back end of the telescope tube surrounding the primary mirror inside the telescope (right).

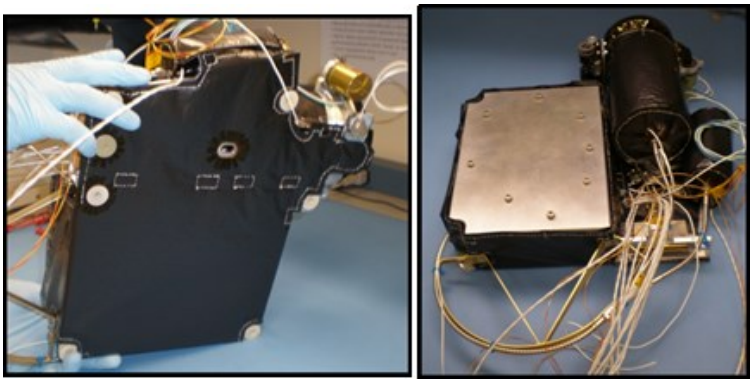

Figure 0-7. The MLI, with a black gallium external layer, covers all three of the UVS components leaving only the harnessing and fiber optic cable exposed.

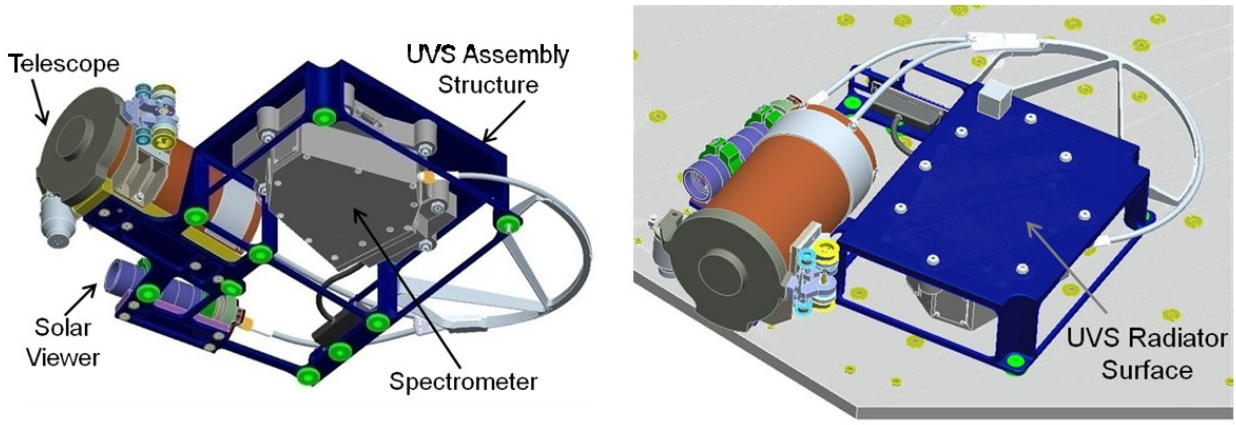

Figure 2-8. The UVS spectrometer is inverted and mounted to the bottom of the assembly structure, flowing heat from the spectrometer out though the radiator surface of the assembly plate.

Frequency (Hz)	ASD Level (g^2/Hz)	
	Qualification	Acceptance
20	0.026	0.013
20-50	+6 dB/oct	+6 dB/oct
50-800	0.16	0.08
800-2000	-6 dB/oct	-6 dB/oct
2000	0.026	0.013
Overall	14.1 G_{rms}	10.0 G_{rms}

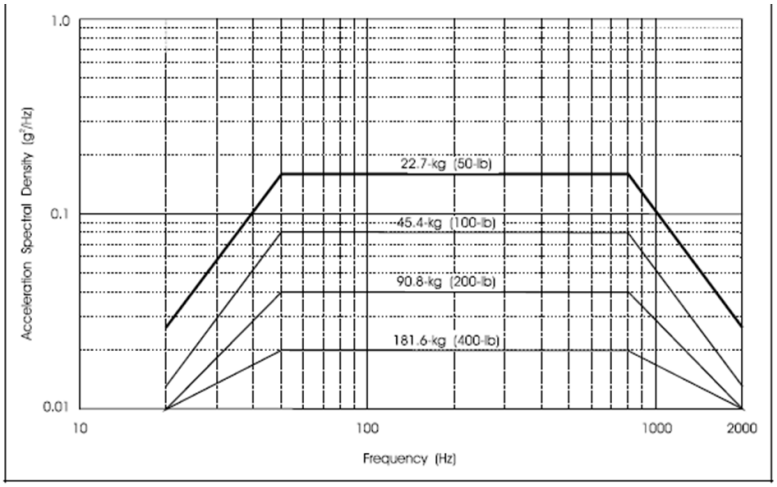

Figure 0-2. UVS was tested to the vibration test levels specified from GEVS.

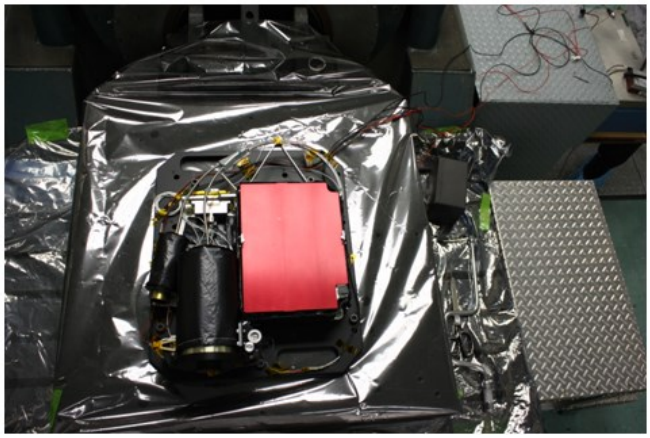

Figure 0-1. The flight UVS instrument was mounted on the vibration table covered in Mylar to prevent any contamination from the table coming in contact with UVS

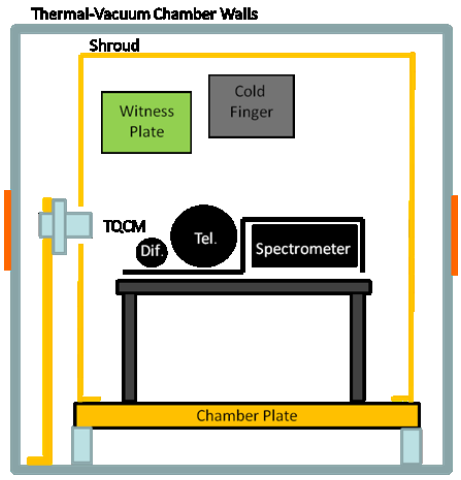

Figure 0-4. This rough block diagram of the UVS thermal test set-up depicts all of the components that were in the chamber during the test.

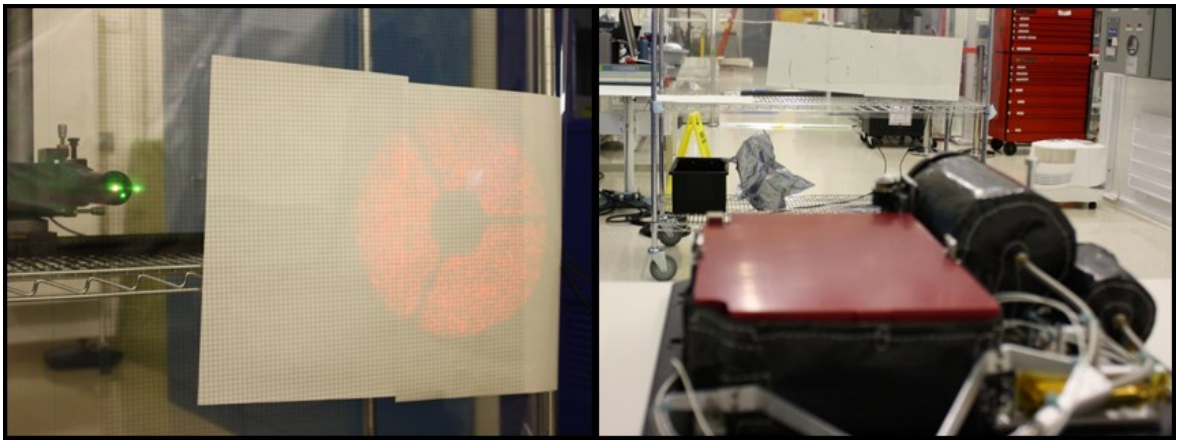

Figure 0-3. (Left) The test grid for FOV telescope measurements was mounted across from the instrument and the FOV was projected on to the target area. (Right) Before projecting the FOV, the instrument was placed on a flat surface and leveled.

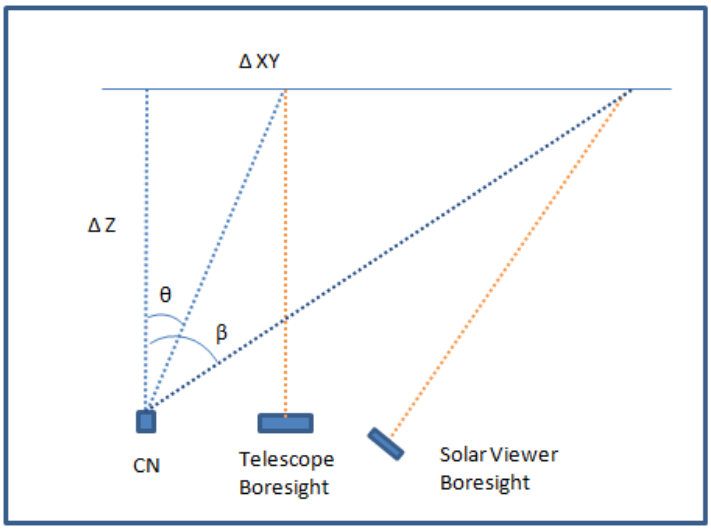

Figure 0-5. Angles θ and β were calculated to determine the offset of the telescope and solar viewer boresight relative to the alignment cube position.

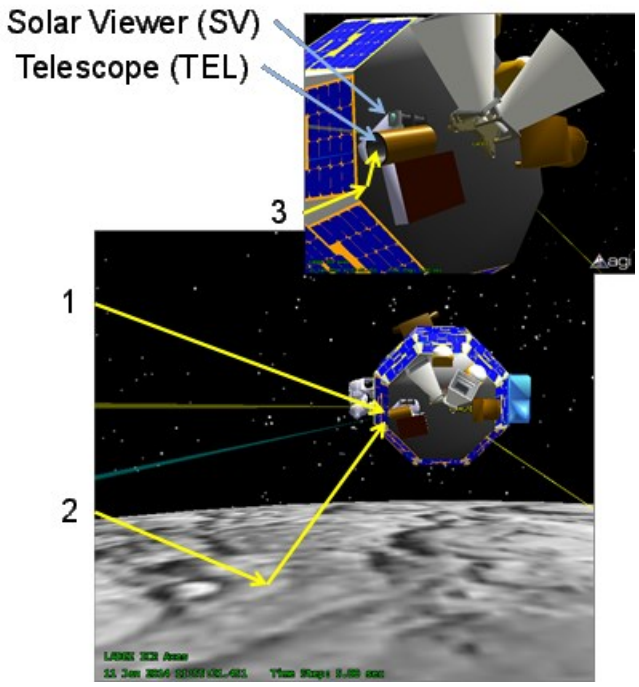

Figure 0-3: Shown are the two primary sources of stray

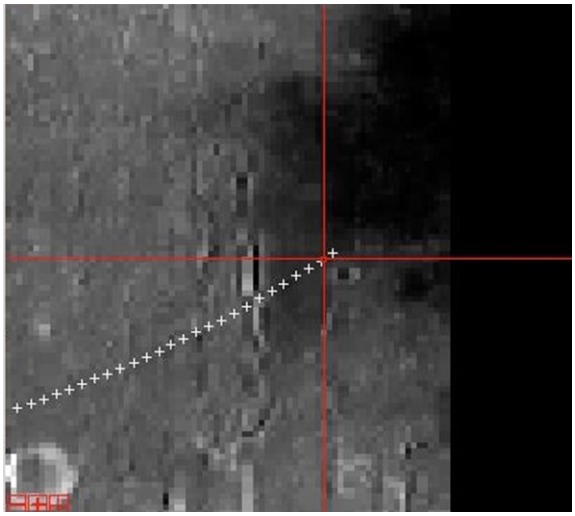

Figure 0-4. The UVS spectral collections (+) were plotted over an M3 image of the same area to determine the overlap in measurements.

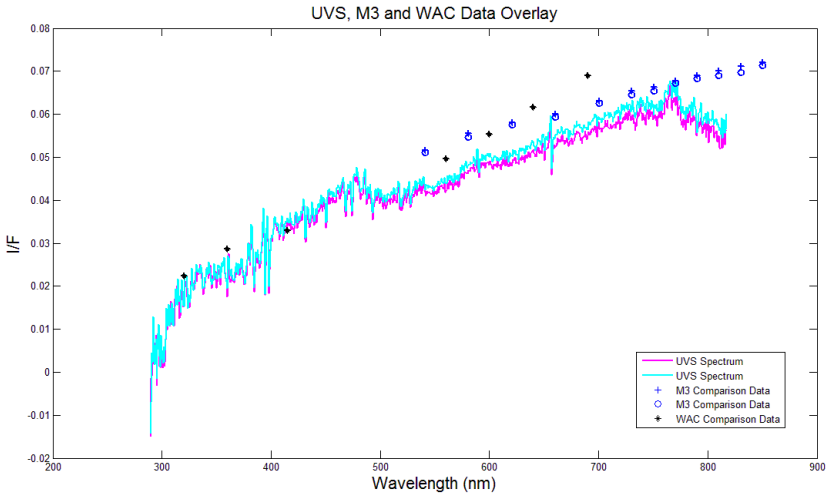

Figure 4-5 A preliminary comparison of M3 and WAC I/F for a single UVS nadir activity.

v

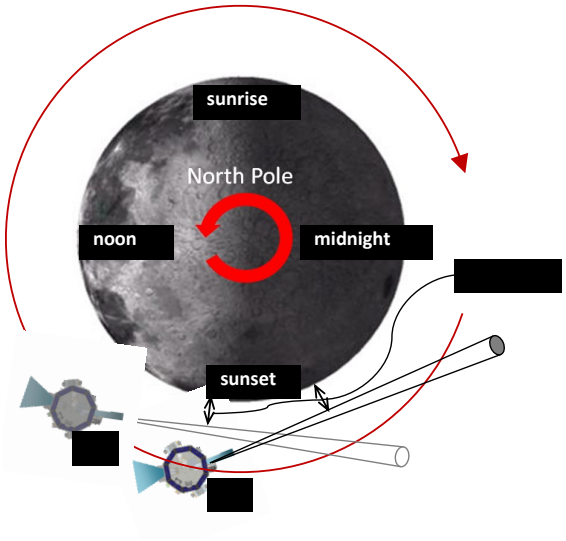

Figure 0-6. Stare portion of limb activity.

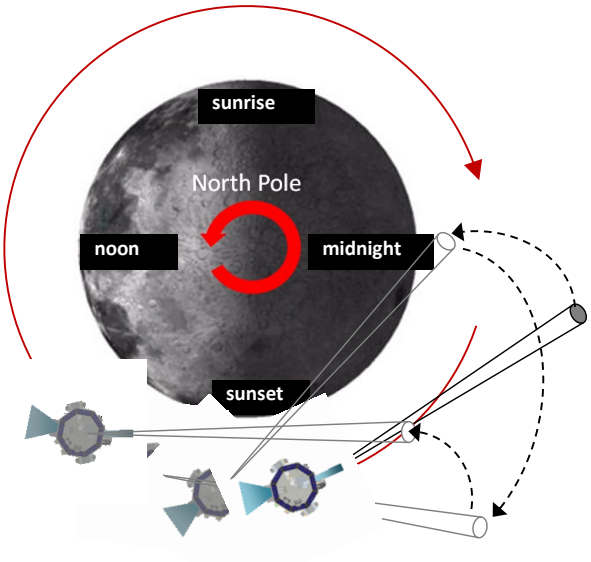

Figure 0-7. Nod portion of limb activity.

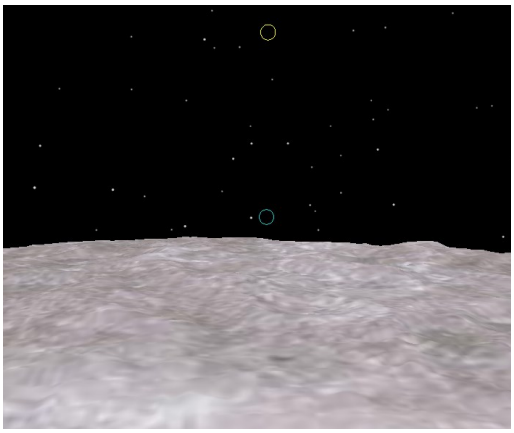

Figure 0-9. Positions of the telescope (blue circle) and solar viewer (yellow circle) fields of view during a limb stare

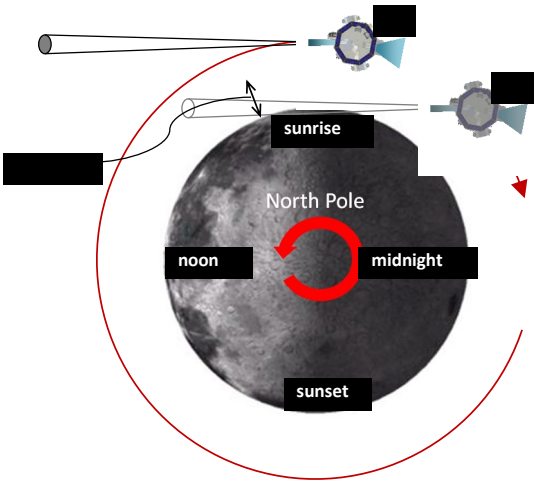

Figure 0-8. Occultation activity.

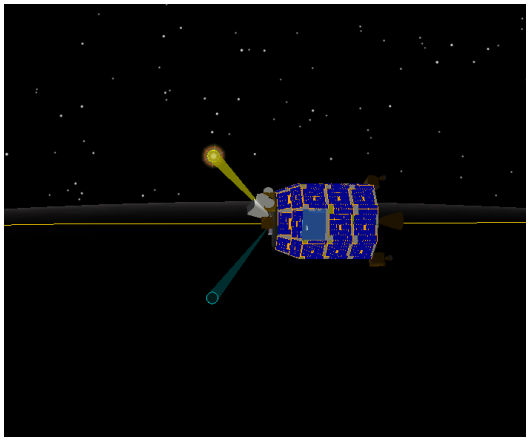

Figure 0-5. Shown is another view of an occultation activity.

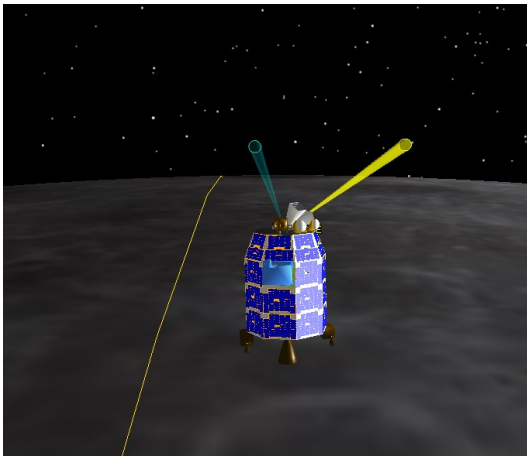

Figure 0-6. North-South Activity

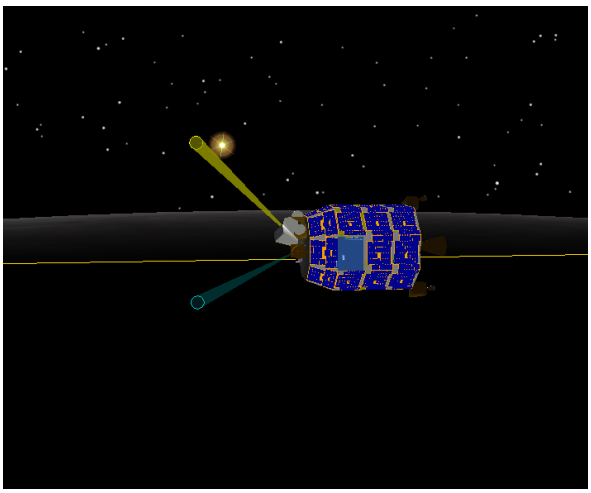

Figure 0-7. Almost Occultation Activity

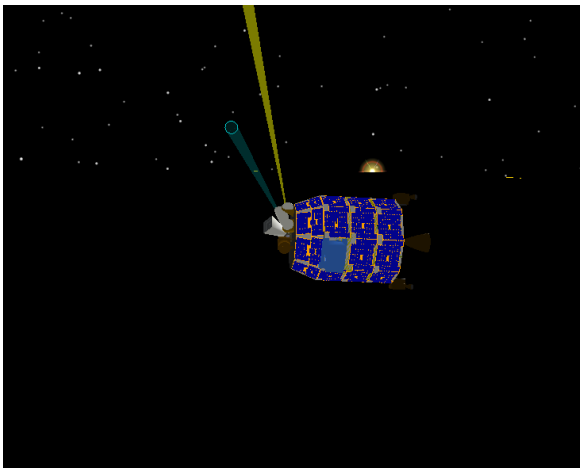

Figure 0-8. Almost Limb Activity

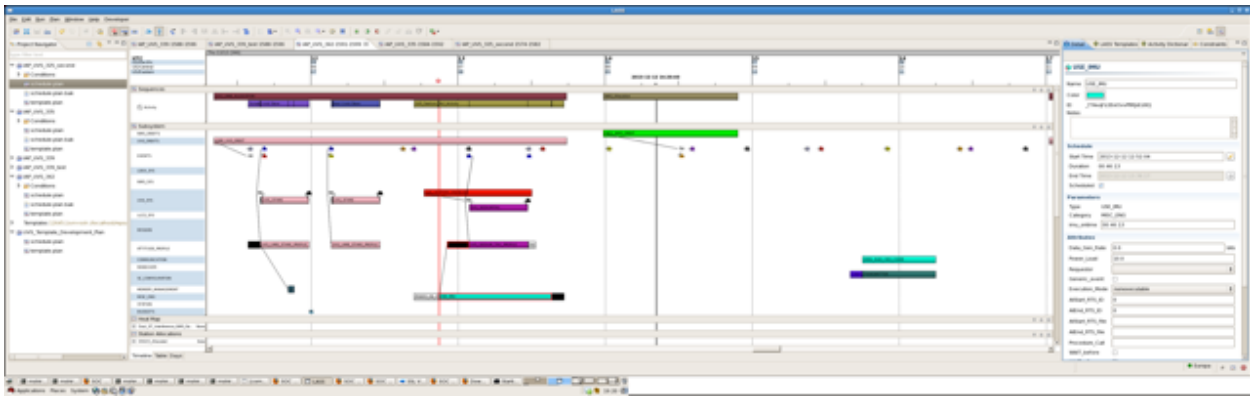

Figure 0-10. LASS was used to insert UVS activities in around other instrument RTSes and spacecraft RTSes.

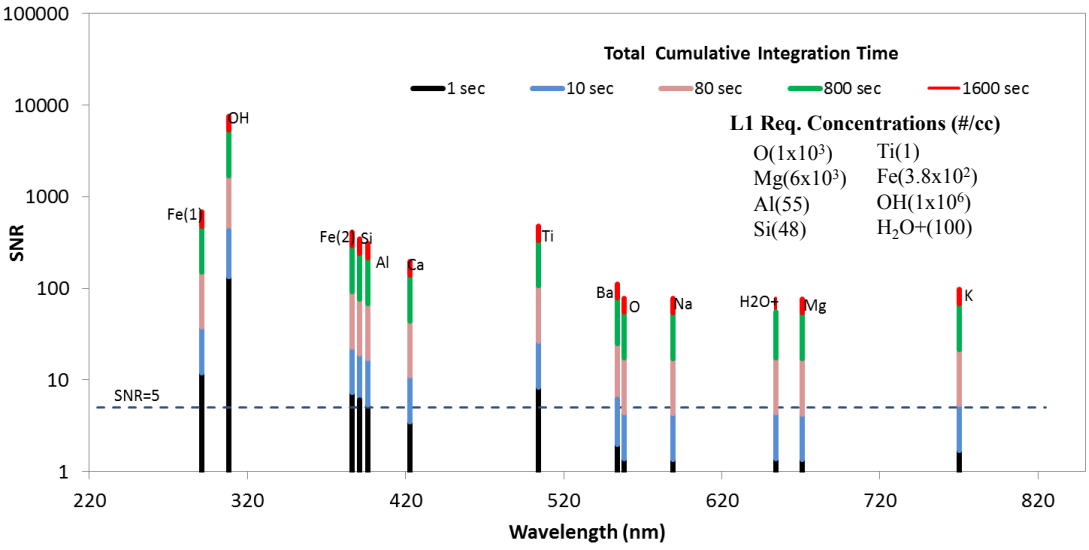

Fig. 5-10 The calculated SNR for several cumulative integration times for the various exospheric gas emission lines estimated for a detector temperature of -20°C. The line strengths were calculated at the specified concentrations in the Level 1 requirement.

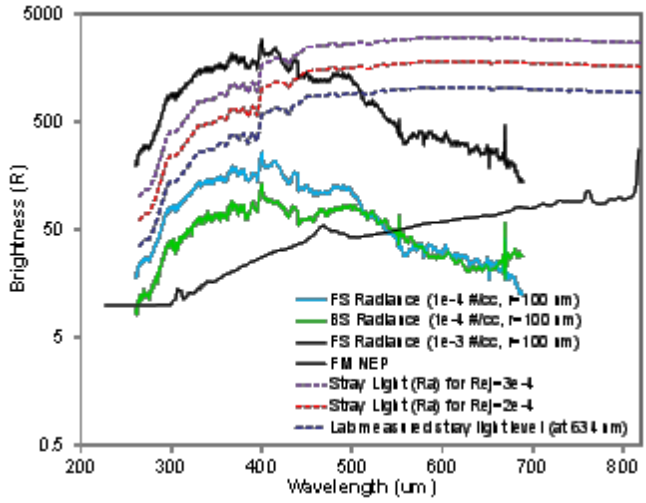

Figure 5-12 Examples of calculated forward and backscatter radiance for dust grains with radii=100 nm (see text for details). Also plotted is the estimated off-axis scattering contribution at a stare altitude of 20 km (Rej = 3e-4) and 50 km (Rej = 2e-4) and the UVS NEP (-20°C).

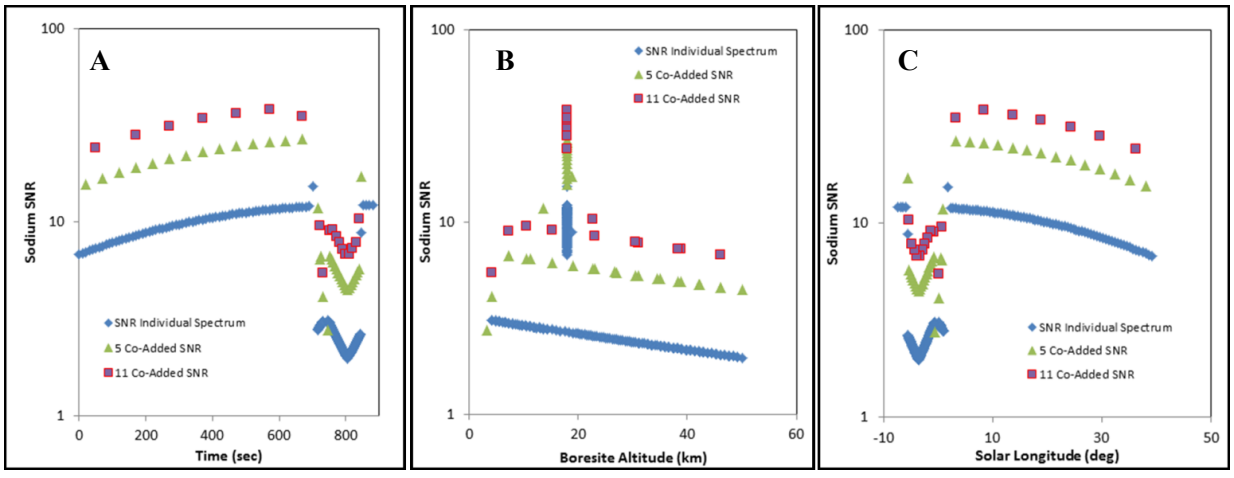

Figure 5-11 Simulations of a UVS "Noon" activity showing the SNR for sodium. (A) The Sodium SNR vs activity time, (B) Sodium SNR vs. telescope boresight altitude, and CB) the Sodium SNR vs. telescope boresight solar longitude.

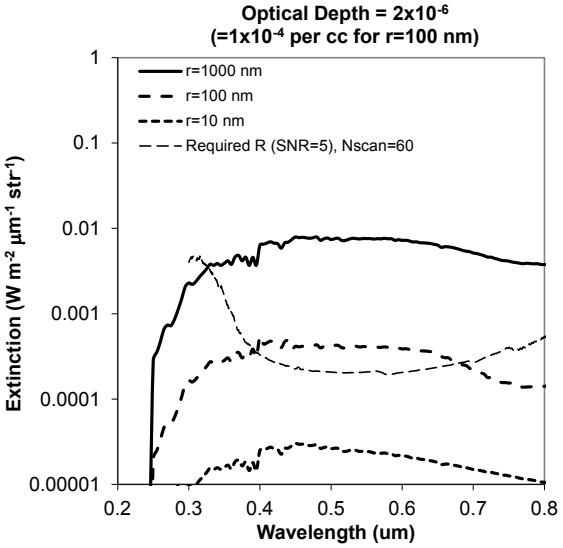

Figure 5-13 Shown is the predicted extinction for three dust grain radii of 10, 100, and 1000 nm at a concentration of 10^{-4} per cc. Also shown is the instrument sensitivity, laboratory measured NEP for a detector at -20°C, but modified to account for in-flight measured increases in noise from radiation effects.